J|A|C|S
ARTICLES
Published on Web 08/08/2006

The True Nature of the Di-iron(III) γ-Keggin Structure in Water: Catalytic Aerobic Oxidation and Chemistry of an Unsymmetrical Trimer

Bogdan Botar,[†] Yurii V. Geletii,[†] Paul Kögerler,[‡] Djamaladdin G. Musaev,[†] Keiji Morokuma,[†] Ira A. Weinstock,*[,§] and Craig L. Hill*[,†]

Contribution from the Department of Chemistry, Emory University, Atlanta, Georgia 30322, Ames Laboratory, Iowa State University, Ames, Iowa 50011, and Department of Chemistry, City College of The City University New York, New York, New York 10031

Received May 5, 2006; E-mail: chill@emory.edu; iaw@sci.ccny.cuny.edu

Abstract: The complex $[\gamma(1,2)\text{-}SiW_{10}\{Fe(OH_2)\}_2O_{38}]^{6-}$ (**1**) has been reported to catalyze the much sought reductant-free selective O_2-based epoxidation of alkenes (Nishiyama, Y.; Nakagawa, Y.; Mizuno, N. *Angew. Chem. Int. Ed.* **2001**, *40*, 3639−3641) in chlorocarbon−acetonitrile solution. The challenge of reproducing catalysis by **1** led us to examine this chemistry in detail. In H_2O, a desirable solvent for catalysis, **1**, does not exist in the proposed organic-medium form in which the two iron atoms are in the binding pocket defined by the equatorial oxygens and, importantly, by two oxygens bound to the central Si heteroatom. Instead, **1** in H_2O initially forms an unusual trimer $[\{Fe_2(OH)_3(H_2O)_2\}_3(\gamma\text{-}SiW_{10}O_{36})_3]^{15-}$ (**2**). The X-ray structure of **2** shows that the $Fe-O_{Si}$ bonds are cleaved and new bonds (μ-hydroxo bridges) form between these Fe centers and those of the neighboring $[\gamma(1,2)\text{-}SiW_{10}Fe_2]$ units. Structural, physical, and computational evidence indicate that if the bonds between the d-electron center, M (Fe in the case of **1** and **2**), and the terminal ligands on M are stronger than the $M-O_x$ bonds, then the out-of-pocket form is more stable and is the one observed. Significantly, **2** in H_2O forms an intermediate that catalyzes the effective aerobic oxidation of sulfur compounds (mercaptoethanol is oxidized to the corresponding disulfide by O_2 at ambient pressure and temperature). All experimental findings are consistent with dissociation of a γ-SiW_{10} Keggin unit from the trimer, **2**, to form the catalytically active species.

Introduction

The development of catalysts for the selective reductant-free oxidation of organic molecules by O_2/air in water, the most environmentally and economically attractive oxidant and solvent, respectively, remains a major goal. Several systems have been reported to catalyze reductant-free O_2-based oxidations that proceed with selectivities that are inconsistent with radical chain oxidation processes (autoxidation). Selective catalytic aerobic epoxidation systems remain as few in number as they are provocative and potentially significant. The initial tetramesityl ruthenium porphyrin (1985)[1] and subsequent polyoxometalate (POM) systems,[2] especially $[(ZnW_9O_{34})_2WZnRu_2(OH)(H_2O)]^{11-}$ [3−5] and $[\gamma(1,2)\text{-}SiW_{10}\{Fe(OH_2)\}_2O_{38}]^{6-}$ (**1**),[6,7] have all garnered considerable attention. Heterolytic (nonradical) catalytic systems for air-only oxidation of sulfur and other compounds have also been developed recently.[8−15] The di-μ-hydroxo/oxo Fe_2 unit in **1** has multiple readily exchangeable ligands on Fe and resides in a ligand environment that readily stabilizes multiple oxidation states of the Fe centers. These features are shared by the heavily investigated active sites of methane monooxygenase (MMO) and ribonucleotide reductase (RNR).[16−18]

[†] Emory University.
[‡] Iowa State University.
[§] City College of The City University New York.

(1) Groves, J. T.; Quinn, R. *J. Am. Chem. Soc.* **1985**, *107*, 5790−5792.
(2) Below is a list of reviews of polyoxometalate catalyzed processes: (a) Hill, C. L. In *Comprehensive Coordination Chemistry II: From Biology to Nanotechnology*; Wedd, A. G., Ed.; Elsevier: Oxford, 2004; Vol. 4, pp 679−759. (b) Neumann, R. In *Transition Metals for Organic Synthesis*, 2nd ed.; Beller, M., Bolm, C., Eds.; Wiley-VCH: Weinheim, 2004; Vol. 2, pp 415−426. (c) Kozhevnikov, I. V. *Catalysis by Polyoxometalates*; Wiley: Chichester, England, 2002; Vol. 2. (d) Moffat, J. B. *Metal−Oxygen Clusters: The Surface and Catalytic Properties of Heteropoly Oxometalates*.; Kluwer Academic/Plenum Publishers: New York, 2001; Vol. 9. (e) Mizuno, N.; Misono, M. *Chem. Rev.* **1998**, *98*, 199−218. (f) Neumann, R. *Prog. Inorg. Chem.* **1998**, *47*, 317−370. (g) Okuhara, T.; Mizuno, N.; Misono, M. *Adv. Catal.* **1996**, *41*, 113−252. (h) Hill, C. L.; Prosser-McCartha, C. M. *Coord. Chem. Rev.* **1995**, *143*, 407−455.
(3) Yin, C.-X.; Finke, R. G. *Inorg. Chem.* **2005**, *44*, 4175−4188.
(4) Neumann, R.; Dahan, M. *Polyhedron* **1998**, *17*, 3557−3564.
(5) Neumann, R.; Dahan, M. *Nature* **1997**, *388*, 353−355.
(6) Nozaki, C.; Kiyoto, I.; Minai, Y.; Misono, M.; Mizuno, N. *Inorg. Chem.* **1999**, *38*, 5724−5729.
(7) Nishiyama, Y.; Nakagawa, Y.; Mizuno, N. *Angew. Chem., Int. Ed.* **2001**, *40*, 3639−3641.
(8) Okun, N.; Tarr, J. C.; Hillesheim, D. A.; Zhang, L.; Hardcastle, K. I.; Hill, C. L. *J. Mol. Catal. A. Chem.* **2006**, *246*, 11−17.
(9) Okun, N. M.; Anderson, T. M.; Hill, C. L. *J. Am. Chem. Soc.* **2003**, *125*, 3194−3195.
(10) Okun, N. M.; Anderson, T. M.; Hardcastle, K. I.; Hill, C. L. *Inorg. Chem.* **2003**, *42*, 6610−6612.
(11) Rhule, J. T.; Neiwert, W. A.; Hardcastle, K. I.; Do, B. T.; Hill, C. L. *J. Am. Chem. Soc.* **2001**, *123*, 12101−12102.
(12) Boring, E.; Geletii, Y. V.; Hill, C. L. *J. Mol. Catal. A: Chem.* **2001**, *176*, 49−63.
(13) Boring, E.; Geletii, Y. V.; Hill, C. L. *J. Am. Chem. Soc.* **2001**, *123*, 1625−1635.
(14) Martín, S. E.; Rossi, L. I. *Tetrahedron Lett.* **2001**, *42*, 7147−7151.
(15) Bosch, E.; Kochi, J. K. *J. Org. Chem.* **1995**, *60*, 3172−3183.

10.1021/ja063157l CCC: $33.50

Since the original synthesis and characterization of [γ-$SiW_{10}O_{36}$]$^{8-}$ by Tézé and co-workers,[19] this di-defect ("di-lacunary") polyoxoanion has been used to prepare a variety of 1,2-di-d-metal-substituted derivatives, [γ(1,2)-SiW_{10}{$M(OH_2)$}$_2$-O_{38}]$^{n-}$, complexes with adjacent d-electron centers, including **1**, and other families of POMs.[20−24] This growing body of work has largely focused on the synthesis, structures, and occasionally magnetic properties of these complexes. The speciation chemistry in solution including that of the catalytically attractive di-iron derivative, **1**, is lacking. We sought to determine the nature of **1** in water and if the reported attractive (high-turnover selective reductant-free O_2-based) epoxidation catalyzed by **1** and other selective O_2-based oxidations might be possible in water versus the decidedly nongreen solvent used to date (dichloromethane−acetonitrile).[7]

We report here that the chemistry of **1** in water is complex with formation of an unusual trimer of **1**, [{$Fe_2(OH)_3(H_2O)_2$}$_3$-(γ-$SiW_{10}O_{36}$)$_3$]$^{15-}$ (**2**) being dominant at early times. The true structure of **1** in water is revealed and involves a different binding motif for the two proximal iron centers than that proposed previously,[6] one in which the bonds between the 3d metals (two Fe centers in this case) and the heteroatom oxygen (O−Si in this case) are cleaved. These "out-of-pocket" structures enable the Fe centers to bridge to other units as in **2**. The physical and structural properties of **2** and other complexes are reported. Although we have not found that **1** catalyzes the reported aerobic epoxidations in organic solvents, we do find that **2** evolves to a species in water that catalyzes the aerobic (air only) oxidation of thiols at ambient temperature in water, a reaction of interest in context with environmental beneficiation, odor abatement and chemical synthesis. Both experimental data (X-ray structures, kinetics, product studies, and spectroscopy) and computational investigations at the DFT level are all consistent and reveal a chemistry, at least in H_2O, in which the active unit is better viewed as an Fe_6 cluster stabilized by three multivalent polyoxotungstate scaffolds than as a di-iron polytungstate, a view distinct from that in any previous study involving d-electron-metal-substituted POMs.

Experimental Section

General Methods and Materials. [γ(1,2)-SiW_{10}{$Fe(OH_2)$}$_2O_{38}$]$^{6-}$, **1**,[6] potassium γ-decatungstosilicate, K_8[γ-$SiW_{10}O_{36}$]·$12H_2O$,[19,25] and [β-$SiFe_2W_{10}O_{36}(OH)_2(H_2O)Cl$]$^{5-}$ (**3**)[26] were prepared according to the literature methods, and their identities and purities were confirmed by infrared spectroscopy. Elemental analyses were performed by Kanti Labs (Mississauga, Canada) and Atlantic Microlab Inc. (Norcross, GA). Infrared spectra (2% sample in KBr) were recorded on a Nicolet 510 FTIR spectrometer. Electronic absorption spectra were recorded on a Hewlett-Packard 8452A diode array spectrophotometer. The circular dichroism (CD) spectra were acquired using a JASCO J-715 spectropolarimeter with 1-mm path length cells; the spectral range was 200−600 nm with a step size of 0.5 nm and a scan speed of 50 nm min^{-1}. ^{29}Si NMR spectra (referenced to 3.6 M TMS in $CDCl_3$) were acquired at room temperature using a UNITY 600FT NMR instrument. To achieve sufficiently concentrated solutions for ^{29}Si NMR, Rb_{11}[{(β-$SiFe_2W_{10}O_{37}(OH)(H_2O)$}$_2$(μ-OH)]·$20H_2O$·0.5RbCl (**Rb4**) was treated with $LiClO_4$, and the resultant insoluble perchlorates were removed by filtration. Differential scanning calorimetric and thermogravimetric data were recorded on ISI DSC 550 and TGA 1000 instruments, respectively. Susceptibility data were measured for **K_7[$(CH_3)_2(NH_2)$]$_8$2** at 0.1, 1.0, and 5.0 T in a temperature range of 2−290 K using a Quantum Design MPMS-5 SQUID magnetometer. These data were corrected for diamagnetic and temperature-independent paramagnetic contributions that were established from standard Pascal constants and measurements of diamagnetic {SiW_{11}}-type Keggin compounds. Small susceptibility differences at lowest temperatures observed for different fields indicate the presence of ∼0.9% mononuclear Fe^{III} complex per formula unit. The range of exchange parameters used in the adaptive fitting procedure covered values from $J/k_B = -50$ to 0 K; nearest-neighbor spin Hamiltonian terms were of the form $-2J\boldsymbol{S}_n\boldsymbol{S}_m$. The changes in the electronic absorption spectra of the Fe-containing POMs were recorded in a gastight optical cell equipped with a stopcock and a rubber stopper sleeve.

Synthesis of K_7[$(CH_3)_2(NH_2)$]$_8$[{$Fe_2(OH)_3(H_2O)_2$}$_3$(γ-$SiW_{10}O_{36}$)$_3$]·$31H_2O$ (K_7[$(CH_3)_2(NH_2)$]$_8$2). Solid $Fe(NO_3)_3$·$9H_2O$ (0.55 g, 1.36 mmol) was added to a solution of K_8[γ-$SiW_{10}O_{36}$]·$12H_2O$ (2.00 g, 0.67 mmol) in 25 mL of H_2O. The solution turned bright yellow in a few seconds, and the pH dropped to ca. 1.8. To this solution, K_2CO_3 (1 M) was added dropwise (ca. 1 mL) until the pH was 4.3. The resulting turbid yellow mixture was stirred for 3 min, and then solid $(CH_3)_2NH_2Cl$ (2.00 g, 12.2 mmol) was added. A yellow precipitate was removed by filtration and the clear filtrate was allowed to stand at room temperature. Yellow-green crystals formed within a few minutes. Yield 0.8 g (40% based on W). IR (2% KBr pellet; 2000−400 cm^{-1}): 1618 (m−w), 1464 (m), 1412 (w), 1028 (m), 1000 (m−w), 951(s), 876 (vs), 793 (vs), 724 (s), 534 (s). UV−vis (fresh solution in H_2O) [λ_{max}, nm (ε, M^{-1} cm^{-1})]: 444 (210), ca. 270 (sh). ^{29}Si NMR (ppm, in D_2O at pH 6): −94.5 ($\delta\nu_{1/2}$ = 25.0 Hz), −96.1 ($\delta\nu_{1/2}$ = 21.0 Hz). Anal. calcd (found) for $W_{30}Fe_6Si_3K_7O_{154}N_8C_{16}H_{147}$: W, 60.44 (60.7); Fe, 3.67 (3.71); Si, 0.92 (0.97); K, 3.00 (2.95); N, 1.23 (1.33); C, 2.11 (2.04).

Synthesis of Rb_{11}[{(β-$SiFe_2W_{10}O_{37}(OH)(H_2O)$}$_2$(μ-OH)]·$20H_2O$·0.5RbCl (Rb4). Complex **4** results from decomposition of **2** in water followed by precipitation with Rb^+. Authentic **4** is prepared as follows. A 1 mM solution of **K_7[$(CH_3)_2(NH_2)$]$_8$2** in 50 mL was kept for 6−7 days in a closed flask. At this stage the UV−vis spectrum indicated the complete disappearance of the λ_{max} = 444 nm band indicative of **2**. Next, the solution was treated with a 5-fold excess of RbCl (0.70 g, 5.8 mmol). Upon addition of RbCl the pH decreased from 6.0 to 4.8. After filtering off a slight cloudiness the solution was left standing at room temperature. Pale yellow-green plate crystals formed after 4−5 days. Yield 0.35 g (70% based on **K_7[$(CH_3)_2(NH_2)$]$_8$2**). IR (2% KBr pellet; 2000−400 cm^{-1}): 1620 (m−w), 994 (m), 954 (s), 897 (vs), 778 (vs), 540 (w,sh). UV−vis [λ_{max}, nm (ε, M^{-1} cm^{-1})]: 465 sh (55), ca. 270 (sh). Anal. calcd (found) for $W_{20}Fe_4Si_2Rb_{11.5}Cl_{0.5}O_{99}H_{47}$: W, 55.81 (55.2); Fe, 3.39 (3.39); Si, 0.85 (1.21); Rb, 14.92 (15.5). ^{29}Si NMR (ppm, in D_2O at pH 4, Li^+ salt in H_2O): no signal.

X-ray Crystallography. Crystals of **K_7[$(CH_3)_2(NH_2)$]$_8$2** and **Rb4** were taken directly from the mother liquor and immediately cooled to 173(2) K on a Bruker D8 SMART APEX CCD sealed tube diffractometer with graphite monochromated (three circle goniometer with 1K CCD detector, Mo−Kα (0.71073 Å) radiation). Structure solution and

(16) Gherman, B. F.; Baik, M.-H.; Lippard, S. J.; Friesner, R. A. *J. Am. Chem. Soc.* **2004**, *126*, 2978−2990.
(17) Baik, M.-H.; Newcomb, M.; Friesner, R. A.; Lippard, S. J. *Chem Rev.* **2003**, *103*, 2385−2419.
(18) Que, L., Jr.; Tolman, W. B. *Angew. Chem., Int. Ed.* **2002**, *41*, 1114−1137.
(19) Canny, J.; Tézé, A.; Thouvenot, R.; Hervé, G. *Inorg. Chem.* **1986**, *25*, 2114−2119.
(20) Bassil, B. S.; Dickman, M. H.; Kortz, U. *Inorg. Chem.* **2006**, *45*, 2394−2396.
(21) Goto, Y.; Kamata, K.; Yamaguchi, K.; Uehara, K.; Hikichi, S.; Mizuno, N. *Inorg. Chem.* **2006**, *45*, 2347−2356.
(22) Kortz, U.; Jeannin, Y. P.; Tézé, A.; Hervé, G.; Isber, S. *Inorg. Chem.* **1999**, *38*, 3670−3675.
(23) Mialane, P.; Dolbecq, A.; Marrot, J.; Rivière, E.; Sécheresse, F. *Chem.−Eur. J.* **2005**, *11*, 1771−1778.
(24) Mialane, P.; Duboc, C.; Marrot, J.; Rivière, E.; Dolbecq, A.; Sécheresse, F. *Chem.−Eur. J.* **2006**, *12*, 1950−1959.
(25) Tézé, A.; Hervé, G. In *Inorganic Syntheses*; Ginsberg, A. P., Ed.; John Wiley and Sons: New York, 1990; Vol. 27, pp 85−96.
(26) Botar, B.; Geletii, Y. V.; Kögerler, P.; Musaev, D. G.; Morokuma, K.; Weinstock, I. A.; Hill, C. L. *Dalton Trans.* **2005**, 2017−2021.

refinement, graphic and generation of publication materials were performed using SHELXTL, V 6.12 software.

Crystal Data for $K_7[(CH_3)_2(NH_2)]_8$2: $W_{30}Fe_6K_7Si_3O_{154}N_8C_{16}H_{147}$, $M = 9124.99$, monoclinic, space group $C2$, $a = 32.062(2)$ Å, $b = 20.3625(14)$ Å, $c = 12.7065(9)$ Å, $\beta = 105.372(2)°$, $V = 7998.9(10)$ Å^3, $Z = 2$, $\rho = 3.789$ g/cm^3, $\mu = 22.320$ mm^{-1}, F (000) = 8164, crystal size = 0.21 × 0.10 × 0.06 mm^3. A total of 72 436 reflections ($1.66 < \Theta < 33.04°$) were collected of which 28 511 reflections were unique (R(int) = 0.0689). $R = 0.0672$ for 22 614 reflections with $I > 2\sigma(I)$, $R = 0.0888$ for all reflections; max/min residual electron density 2.65 and −3.03 e Å^{-3}. **Crystal Data for Rb4:** $W_{20}Fe_4Si_2Rb_{11.5}Cl_{0.5}O_{99}H_{47}$, $M = 6588.59$, triclinic, space group $P\bar{1}$, (no. 2), $a = 12.4883(8)$ Å, $b = 18.783(1)$ Å, $c = 20.833(1)$ Å, $\alpha = 98.777(1)$, $\beta = 101.797(1)$, $\gamma = 94.181(2)$, $V = 4700.0(5)$ Å^3, $Z = 2$, $\rho = 4.656$ g/cm^3, $\mu = 31.035$ mm^{-1}, F (000) = 5770, crystal size = 0.15 × 0.08 × 0.04 mm^3. A total of 49 364 reflections ($1.62 < \Theta < 28.33°$) were collected of which 23 280 reflections were unique (R(int) = 0.0486). $R = 0.0449$ for 19 077 reflections with $I > 2\sigma(I)$, $R = 0.0597$ for all reflections; max/min residual electron density 5.11 and −4.43 e Å^{-3}.

Computational Procedures. All calculations were performed using the Gaussian 03 program.[27] The geometries of these species were optimized without any symmetry constraints at the B3LYP/Lanl2dz level of theory with additional d-polarization functions for Si atom ($\alpha = 0.55$) and the corresponding Hay-Wadt effective core potential (ECP) for W.[27−29]

Reactivity Studies. All chemicals in these studies were commercial or synthesized according to the literature procedures.

Cyclooctene Oxidation. The reaction was carried out in 20-mL pressure vessels with an internal thread for use with a PTFE bushing as a pressure seal. A desired amount of a solid catalyst was placed into a vessel purged with O_2 or air, then 3−4 mL of a solution containing cyclooctene, acetonitrile, dichloroethane (or other cosolvents), and 1,3-dichlorobenzene (an internal standard for GC-analysis) was added. The reaction vessel was sealed and placed into a thermostated oil-bath (84 ± 1 °C). At set time intervals, the vessel was cooled to 0 °C, opened, and a small aliqout (∼0.05 mL) was withdrawn. This aliquot was diluted with EtOH for GC analysis. The reaction vessel at 0 °C was purged with O_2 (or air), sealed and placed again in the oil-bath. The cyclooctene oxidation products (cyclooctene oxide, 1-cyclooctene-2-ol, and 1-cyclooctene-2-one) were identified and quantified using gas chromatography with internal standard techniques.

2-Mercaptoethanol Oxidation. The catalytic reactions were carried out in 28-mL glass vials with aluminum seals and PTFE/silicon septa under vigorous agitation with a magnetic stirring bar at ambient temperature (24 ± 1 °C). The vials were carefully purged with dioxygen or with air before use. The catalyst was dissolved in 2−3 mL of water (or other solvent) containing a required amount of RSH and the reaction started. At desired time intervals, an aliquot of the reaction mixture (10−20 mL) was withdrawn with a Hamilton microliter syringe and the RSH concentration was quantified. The data were plotted as RSH concentration versus time. Thiol was quantified using Ellman's reagent as described in the Supporting Information (SI), and bis(2-hydroxyethyl) disulfide (RSSR) was quantified by ^{1}H NMR. For the latter analyses, spectra were collected on a INOVA 600 MHz NMR spectrometer at ambient temperature and samples were prepared by mixing an aliquot of the reaction mixture (RSH + RSSR) in acidic D_2O (pD = 1.9). Methanol (dissolved in D_2O) was used as an internal standard. Acidic D_2O was used to stop the catalytic reaction: thiol oxidation does not take place at low pH and can be stopped by addition of HCl (ca. 12 M solution in D_2O). The ^{1}H NMR spectrum of the RSH shows two triplets (δ in ppm): 2.66 (br, 2H adjacent to SH) and 3.68 (s, 2H adjacent to OH), and that of RSSR: 2.88 (s, 4H near SH group,) and 3.85 (s, 4H near OH group).

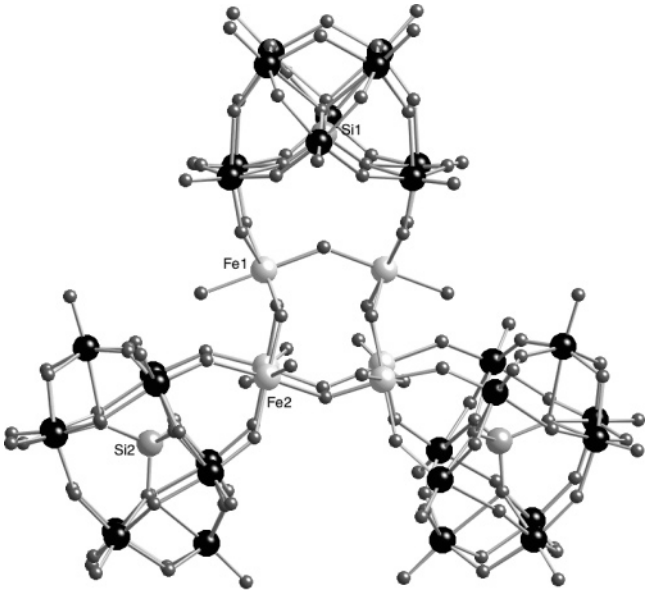

Figure 1. Structure of polyanion **2** in ball-and-stick representation (view perpendicular to the anion's C_2 axis): (W: large black spheres; Fe and Si: large light gray sphere; O: small gray spheres).

H_2O_2 Measurements. H_2O_2 was quantified using $H_5TiPW_{11}O_{40}$ in H_2SO_4 according to Maksimov and co-workers[30] as described in the SI.

Determination of Reaction Stoichiometry. The reaction was carried out in a two-neck round-bottom flask immersed in a water bath to minimize the temperature changes during the reaction (24 ± 0.3 °C). The reaction volume was 15 mL, whereas the headspace volume was ∼22 mL. One neck was attached to a digital manometer to follow dioxygen consumption by monitoring the pressure. A desired amount of solid catalyst was placed into a flask purged with dioxygen and then the flask was sealed with a rubber septum. After thermal equilibration, a 15-mL aliquot of an aqueous solution of RSH (46 mM) was injected into the flask through a rubber septum. Initially, the excess of pressure was released via a needle in a septum which was then removed. At required times, a 1-mL aliquot was withdrawn and the concentrations of RSH, RSSR, and H_2O_2 were determined as described above.

Results and Discussion

Structure of γ-Di-Iron Keggin POMs. The reaction of $[\gamma\text{-}SiW_{10}O_{36}]^{8-}$ with 2 equiv of Fe(III) in aqueous solution at pH 4.3 and ambient temperature followed by addition of a hydrogen bonding cation leads to the immediate formation, not of **1**, but of a new trimeric γ-di-iron(III) polytungstosilicate, $[\{Fe_2(OH)_3(H_2O)_2\}_3(\gamma\text{-}SiW_{10}O_{36})_3]^{15-}$ (**2**) (Figure 1). Polyanion **2** can be viewed as a trigonal (trilobal) arrangement of the three $\{\gamma\text{-}SiW_{10}\}$ units connected by an electrophilic $[Fe_6(OH)_9(H_2O)_6]^{9+}$ central core. The six Fe(III) centers define (span) the corners of a trigonal prism, and each is octahedrally coordinated, sharing two equatorial oxygen atoms with the neighboring SiW_{10} unit.

On the basis of bond valence sum (BVS) calculations, all oxygen atoms bridging the hexanuclear iron core are monoprotonated with values of 1.01−1.18. The small BVS values of the terminal oxygen positions (0.36 to 0.42) bound to the Fe(III) centers are consistent with these being aqua ligands. The $Si(1)W_{10}$ unit is rotated by 90° around the crystallographic C_2

(27) Frisch, M. J. et al. *Gaussian 2003*; Gaussian, Inc.: Pittsburgh, PA 2003.
(28) Becke, A. D. *Phys. Rev. A: At., Mol., Opt. Phys.* **1988**, *38*, 3098−3107.
(29) Hay, P. J.; Wadt, W. R. *J. Chem. Phys.* **1985**, *82*, 270−283.
(30) Maksimov, G. M.; Kuznetsova, L. I.; Matveev, K. I.; Maksimovskaya, R. I. *Koord. Khim.* **1985**, *11*, 1353−1357.

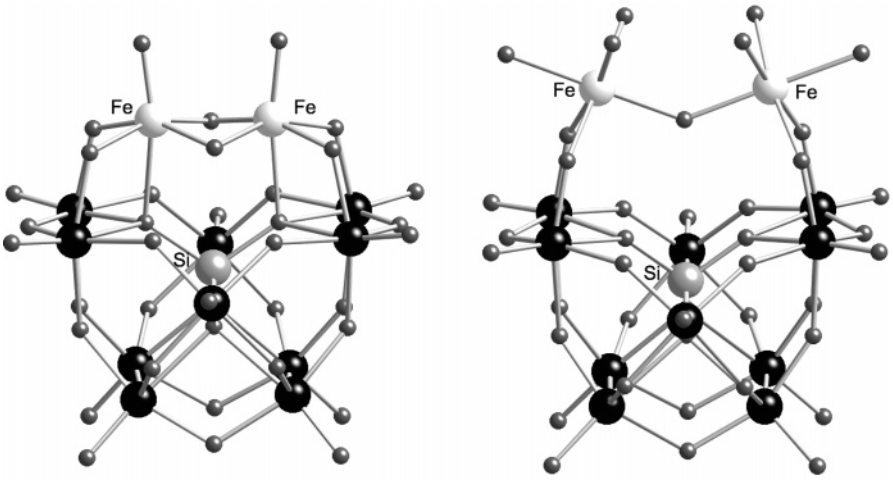

Figure 2. Ball-and-stick illustrations of the in-pocket (left) and the out-of-pocket (right) {γ-$SiW_{10}Fe_2$} monomeric Keggin building unit of **2**.

axis with respect to the other two polyanion units. This is in stark contrast to other trimeric heteropolytungstate assemblies in which the polytungstate fragments lie on a mirror plane.[31−33] The dihedral angle of the least-squares planes defined by [O(21), Si(1), O(10), and Fe(1)] and [Fe1,W6, Si2, and W9] is 3.5° (see Figure S1 in SI). This indicates that two Si(2)W10 units are slightly twisted around the crystallographic C_2 axis from the eclipsed position, rendering the anion chiral (**2** crystallizes in the monoclinic, chiral *C2* space group). The CD spectra of **2** indicates, as expected, that the chirality observed in the crystals is lost when the crystals are dissolved (a 2×10^{-4} M solution of $\mathbf{K_7[(CH_3)_2(NH_2)]_8}$**2** in H_2O shows no optical activity).[34]

Significantly, the two ferric centers in **1** are in the binding pocket and edge sharing, whereas these centers in **2** are out of the binding pocket and corner sharing. The two binding modes (in- and out-of-pocket) are illustrated in Figure 2. The binding pocket is defined by the 5 bridging oxygens in each of the adjacent defect (lacunary) sites on the polytungstate ligand. The in-pocket structure has both Fe(III) centers bound to the internal oxygens on the central heteroatom (Si) in addition to the 4 oxygens in the equatorial plane and the terminal ligand (Figure 2). Cleavage of the Fe−O(Si) bonds results in movement of the Fe atoms out of this pocket. The in-pocket coordination mode for γ-disubstituted Keggin units has been structurally (crystallographically) confirmed by Pope and co-workers for the $Mn(III)_2$ derivative[35] and is certainly reasonable for a range of metals of both larger and somewhat smaller radii than d^4 high-spin Mn(III) (ca. 0.66 Å).[36] This $Mn(III)_2$ complex was crystallized from nonaqueous media (CH_3CN). At the same time, however, there is only one documented example of a di-substituted γ-Keggin complex involving first row transition metals that are out-of-pocket, the $Cr(III)_2$ derivative, [γ(1,2)-$SiW_{10}O_{36}\{Cr(OH_2)(OAc)\}_2]^{5-}$.[37] The coordination positions on Cr that are freed by the movement of Cr out of the pocket (cleaving the Cr−O(Si) bonds) are filled by acetate ligands. It should be noted that this $Cr(III)_2$ derivative has been crystallized from both H_2O and an aprotic organic medium, CH_3CN.

The out-of-pocket structural motif should be energetically reasonable in the presence of ligands of comparable strength to that of the polydentate lacunary ligand of the polytungstate, [γ-$SiW_{10}O_{36}]^{8-}$, itself. Ligand(s) with substantially greater binding constants for the d-electron metal ions than the polytungstate (acetate or likely stronger ligands than acetate) would thermodynamically remove these ions from the polytungstate (complete demetalation). The movement of the two proximal redox active d-metal ions in and out of the polytungstate binding pocket, i.e., ligated to the heteroatom oxygen or not (effectively interconversion of the Figure 2 structures) should be easily affected by changes in reaction conditions and is imminently reasonable mechanistically (indeed a path of least motion). The location of the two adjacent d-electron metal centers in these di-d-metal-center POMs with respect to the pocket could underlie catalytic activity (O_2 and/or substrate binding, etc.) and other properties (magnetism, thermochromism, etc.), of this family of POMs. As a consequence, the electronic structures of a series of [γ(1,2)-$SiW_{10}\{M(OH_2)\}_2O_{38}]^{6-}$, M = 3d or 4d metals, were investigated computationally at the DFT level and these studies found that the in-pocket or out-of-pocket placement of the d-electron metals impacts electronic structure (spin state, etc.), magnetic properties, and other attributes of importance in the above phenomena and applications.[38−40]

The data of Mizuno and co-workers on **1,** which argue in favor of an in-pocket Fe^{III}_2 structure while quite thorough in aggregate, cannot unequivocally rule out the out-of-pocket

(31) Weakley, T. J. R. *J. Chem. Soc., Chem. Commun.* **1984**, 1406−1407.
(32) Botar, B.; Yamase, T.; Ishikawa, E. *Inorg. Chem. Commun.* **2000**, *3*, 579−584.
(33) Kim, K.-C.; Pope, M. T. *Dalton Trans.* **2001**, 986−990.
(34) Chiral POMs that retain their structures in solution, i.e., those that are resistant to isomerization and equilibration upon dissolution, are typically racemic in both solution and in the solid state. There are examples of induced chirality in POMs (the Pfeiffer effect) ((a) Nomiya, K.; Miwa, M.; Sugaya, Y. *Polyhedron* **1984**, *3*, 381−383. (b) Nomiya, K.; Kobayashi, R.; Miwa, M. *Bull. Chem. Soc. Jp.* **1983**, *56*, 3505−3506. (c) Garvey, J. F.; Pope, M. T. *Inorg. Chem.* **1978**, *17*, 1115−1118), a few examples of enantiomerically enriched POMs ((d) Kortz, U.; Matta, S. *Inorg. Chem.* **2001**, *40*, 815−817), and recently some enantiopure POMs ((e) Fang, X.; Anderson, T. M.; Hill, C. L. *Angew. Chem., Int. Ed.* **2005**, *44*, 3540−3544. (f) Fang, X.; Anderson, T. M.; Hou, Y.; Hill, C. L. *Chem. Commun.* **2005**, 5044−5046).
(35) Zhang, X. Y.; O'Connor, C. J.; Jameson, G. B.; Pope, M. T. *Inorg. Chem.* **1996**, *35*, 30−34.
(36) Shannon, R. D.; Prewitt, C. T. *Acta Crystallogr.* **1969**, *B25*, 925−946.
(37) Wassermann, K.; Lunk, H.-J.; Palm, R.; Fuchs, J.; Steinfeldt, N.; Stösser, R.; Pope, M. T. *Inorg. Chem.* **1996**, *35*, 3273−3279.
(38) Musaev, D. G.; Morokuma, K.; Geletii, Y. V.; Hill, C. L. *Inorg. Chem.* **2004**, *43*, 7702−7708.
(39) Quiñonero, D.; Wang, Y.; Morokuma, K.; Khavrutskii, L. A.; Botar, B.; Geletii, Y. V.; Hill, C. L.; Musaev, D. G. *J. Phys. Chem. B.* **2006**, *110*, 170−173.
(40) Zueva, E. M.; Chermette, H.; Borshch, S. A. *Inorg. Chem.* **2004**, *43*, 2834−2844.

Table 1. Calculated Geometry Parameters (in Å) of the Complexes $[\gamma(1,2)\text{-}SiW_{10}\{Fe(L)\}_2O_{38}]^{n-}$, where $n = 4$ for L = None and H_2O (**1**), and $n = 6$ for L = Cl^-, CN^-, and OH^-

parameters	L = none	L = H_2O	L = CN^-	L = Cl^-	L = OH^-
distances:					
Fe^1-Fe^2	2.969	2.985	3.032	3.052	3.112
$Fe^1-O_b{}^1$	2.010	2.020	2.033	2.022	2.031
$Fe^1-O_{Si}{}^1$	2.046	2.050	3.139	3.164	2.793
$Fe^1-O_W{}^1$	1.902	1.897	1.922	1.926	1.966
Fe^1-L^a	–	3.346	2.254	2.543	1.953

[a] The Fe−O and Fe−C distances for L = OH_2, OH, and CN, respectively, are given.

Scheme 1

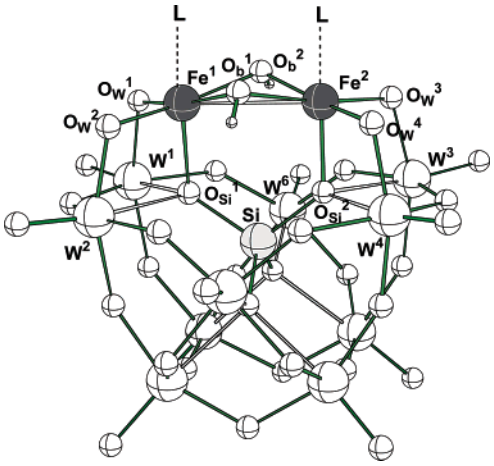

structure (Figure 2). In addition, repeated efforts by the Mizuno group and our group to obtain diffraction quality crystals of **1** from organic media, including the one used in the reported catalytic aerobic epoxidation chemistry (acetonitrile-dichloromethane), have thus far been unsuccessful. It is now clear, however, from the structure of **2** and other data below that **1** in aqueous solution exists in the out-of-pocket form.

Computational Studies. Several central points in this chemistry were addressed computationally at the B3LYP/Lanl2dz level of theory. Table 1 gives the calculated values of key geometry parameters (in Å) of the complexes $[\gamma(1,2)\text{-}SiW_{10}\{Fe(L)\}_2O_{38}]^{n-}$, where $n = 4$ for the terminal ligand, L = none and H_2O, and $n = 6$ for L = Cl^-, CN^-, and OH^- (the labeling and location of atoms and the terminal ligand, L, are given in Scheme 1). L = "none" refers to five-coordinate Fe centers (no terminal ligand on Fe), and L = H_2O is complex **1**.

The calculated geometry parameters of these systems in their high-spin $^{11}A_1$ states are given in Table 1. As seen from this table, the Fe−O(Si) bond distance is found to be 2.046 Å for the complex with no terminal ligands on the Fe centers (L = none). This distance is consistent with a reasonably strong Fe−O(Si) bond and defines the in-pocket structure. Inclusion of two terminal aqua ligands (L = H_2O) into the calculations (which is complex **1**) does not change the geometrical parameters of the system, indicating the lack of (or a very weak) interaction between the Fe centers and their terminal aqua ligands. The calculated $Fe-OH_2$ and Fe−O(Si) distances are 3.346 and 2.050 Å, respectively, which again define the in-pocket structure. However, for the POMs with terminal ligands, L = OH^-, CN^-, and Cl^-, there are both substantial interactions between the Fe centers and these ligands (the calculated Fe−L bond distances are 1.953, 2.254, and 2.543 Å, respectively) and very weak or nonexistent Fe−O(Si) interactions that define the out-of-pocket structure (the calculated Fe−O(Si) distances of 2.793, 3.139, and 3.164 Å, for L = OH^-, CN^-, and Cl^-, respectively). These calculations and the structural data on **2** indicate that the Fe−O bonds in the Fe−OH−Fe units that bridge the different γ-Keggin POM units in the trimer, **2**, are stronger than the terminal $Fe-OH_2$ bonds but comparable to or weaker than the terminal Fe−OH bonds.

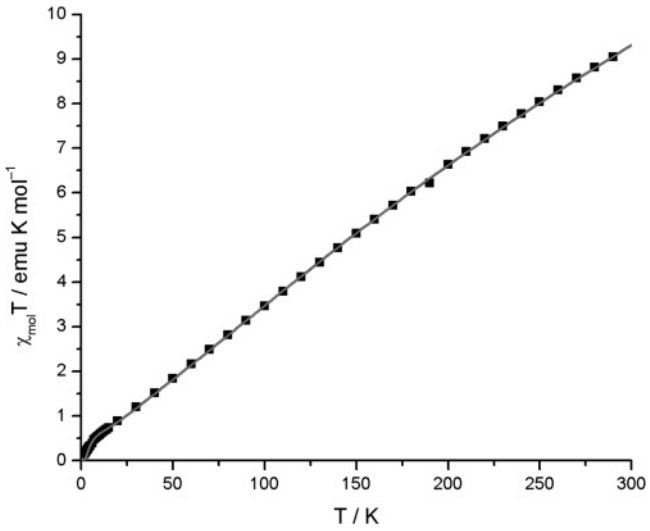

Figure 3. Temperature dependence of χT for **2** at an external field of 0.1 T. Experimental values, corrected for diamagnetic, and TIP contributions are shown as squares, and the best fit for the proposed Heisenberg model (see text) is shown as a gray line.

Magnetic Properties of the Hexa-Iron POM Trimer, 2. Given the potential significance of the structurally unique trimer, **2**, in catalytic aerobic oxidation and other chemistries, we sought to characterize its electronic and magnetic properties in more detail. Because **2** rearranges slowly to other POMs in aqueous solution (discussed in reactivity section below), the magnetic measurements, like the X-ray structures and several other physical measurements, were conducted on the solid (pure crystalline samples in this case).

Three lines of evidence establish that all the iron centers in **2** are in the 3+ oxidation state: (1) the complex was made with hydrated $Fe(NO_3)_3$ exposed to the air (no ferrous iron was present at any time); (2) the collective bond lengths (i.e., BVS calculations) are consistent with Fe(III), not Fe(II); and (3) the magnetic properties, addressed immediately below, also indicate the presence of Fe(III), not Fe(II). A fourth and obvious technique for the assignment of Fe oxidation states, namely ^{57}Fe Mössbauer spectra of **2**, was attempted but scattering from the many tungsten atoms in the complex precluded acquisition of satisfactory data, a situation we have encountered with other Fe-containing polyoxotungstates[41,42] but not the less electron-dense polymolybdates.[43]

The magnetic properties of **2** are characterized by antiferromagnetic coupling between the six $s = 5/2$ Fe^{III} centers of the prismatic cluster anion $\{Fe_6(\mu\text{-}OH)_9(H_2O)_6\}$ core (Figure 3). The intramolecular exchange is solely mediated by the single

(41) Zhang, X.; Chen, Q.; Duncan, D. C.; Campana, C.; Hill, C. L. *Inorg. Chem.* **1997**, *36*, 4208−4215.
(42) Zhang, X.; Chen, Q.; Duncan, D. C.; Lachicotte, R. J.; Hill, C. L. *Inorg. Chem.* **1997**, *36*, 4381−4386.
(43) Botar, B.; Kögerler, P.; Müller, A.; Garcia-Serres, R.; Hill, C. L. *Chem. Commun.* **2005**, 5621−5623.

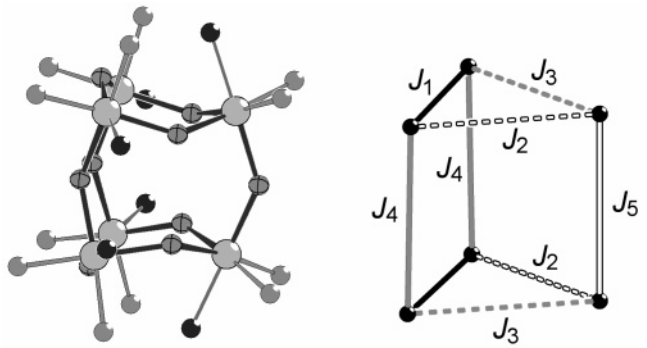

Figure 4. (Left) Ball-and-stick representation of the central $\{Fe^{III}_6\}$ motif of **2** (Fe: large, bright gray spheres; μ-oxo positions of OH groups: crossed gray; oxo positions of terminal H_2O ligands: dark gray; oxo positions of the three coordinated $\{SiW_{10}\}$ fragments: gray). The Fe−OH−Fe bonds, relevant for the intramolecular magnetic superexchange, are highlighted in dark gray. (Right) Corresponding exchange coupling scheme with the assigned five exchange constants, reflecting the C_2 symmetry of the central $\{Fe_6(OH)_9(H_2O)_6\}$ fragment.

μ-hydroxo groups that connect the nearest-neighbor iron positions. Based on the C_2 symmetry of the $\{Fe_6(\mu\text{-}OH)_9(H_2O)_6\}$ core, an isotropic Heisenberg model was adopted that employs five exchange constants (J_1−J_5) for the nine nearest-neighbor interactions to account for the five different geometries of the Fe−OH−Fe bridges (Figure 4). A full computational simulation of this parameter space yielded a best fit to the low-field susceptibility data for $J_1/k_B = -32.5$ K, $J_2/k_B = -30.1$ K, $J_3/k_B = -39.3$ K, $J_4/k_B = -18.6$ K, and $J_5/k_B = -18.7$ K with an isotropic splitting factor $g_{iso} = 2.0$ and resulting in an $S = 0$ ground state. These values correlate well with the predictions from structure−property relations based on their geometric parameters.[44−46] They explain the relative increase in J_3, compared to J_1 and J_2, with a corresponding decrease in the Fe−OH−Fe bond angle to 134 from 140 and 139°, respectively. However, such generalized models fail to explain the pronounced differences between the intratriangle ($J_1/J_2/J_3$) and the intertriangle (J_4/J_5) exchange constants. These results also predict the first zero-temperature field-induced spin-level crossing (from an $S = 0$, $M_s = 0$ state to an $S = 1$, $M_s = -1$) at 6.8 T, which might be probed in the future by high-field magnetization measurements as an independent verification of the proposed model.

Reactivity of 2 in Solution. It is generally prudent and frequently necessary to establish the reactivity and speciation (isomerizations, rearrangements, or decomposition) of a catalyst in solution before an attempt is made to establish the catalytic mechanism in that medium. Once we established the physical and electronic structure of **2**, we focused on elucidating its reactivity in H_2O.

The ^{29}Si NMR spectrum of a freshly prepared solution of **$K_7[(CH_3)_2(NH_2)]_8$2** (30 mM) (Figure 5) shows two signals at −94.5 and −96.0 ppm with an intensity ratio of 2:1, fully consistent with the solid-state structure. However, after ca. 2 h, a new signal appears at −98.3 ppm, which grows in intensity at the expense of the initial two peaks reaching, after 24 h, an intensity similar to that of the initial −96.0 ppm signal. After 15 days, the two signals characteristic of the fresh solution of

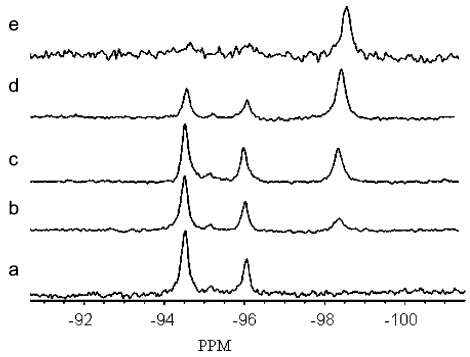

Figure 5. Time dependence of ^{29}Si NMR spectrum of a 30 mM solution of **$K_7[(CH_3)_2(NH_2)]_8$2** in aqueous solution: (a) fresh solution; (b) 8 h; (c) 24 h; (d) 6 days; (e) 15 days. Spectrum e remains virtually unchanged after 40 days.

2 are effectively absent and the −98.3 ppm signal is the only feature of the spectrum (Figure 5). At this point, the solution does not undergo any further change; the spectrum of a solution kept for 40 days is identical to that of one kept 15 days. Evaporation of aged solutions of **$K_7[(CH_3)_2(NH_2)]_8$2** (concentrations of 0.5−30 mM) at room temperature yields, in all cases, an orange-red complex, **5**, which produces the same single-peak ^{29}Si NMR spectrum when redissolved in H_2O. Clearly, **5** has the same metal ion elemental composition of **2** because no action was taken except to age and then remove the H_2O solvent. Despite considerable efforts, **5** failed to crystallize.

The instability of **2** in aqueous solutions is further confirmed by UV−vis spectroscopy (Figure S2). The UV−vis spectrum of a fresh solution of **$K_7[(CH_3)_2(NH_2)]_8$2** shows a characteristic peak at 444 nm ($\epsilon = 210 \pm 10$ M^{-1} cm^{-1}) arising from Fe d−d transitions. The λ_{max} at 444 nm disappears with time and is replaced by a broad shoulder at ca. 400−550 nm (Figure S2). The initial rates of this transformation linearly increase with [**2**] (Figure S4), but then the reaction slows down (deviates from exponential behavior, Figure S3). Such a deceleration is more pronounced for concentrated solutions of **2**. For example, the characteristic peak at 444 nm decreases by a factor of ca. two in 90−100 min for a 30 mM solution versus 40−45 min for a 5 mM solution. A systematic kinetic study to be published elsewhere reveals that this transformation is inhibited by potassium cations, the counterions in **2**, and does not obey a simple exponential law.

Although attempts to isolate a crystalline material directly from solutions of **$K_7[(CH_3)_2(NH_2)]_8$2** (aged until no further changes were apparent in the electronic absorption spectra) were unsuccessful, addition of RbCl to a 1 mM aged solution of **$K_7[(CH_3)_2(NH_2)]_8$2** did produce crystals in a 70−75% yield. The X-ray structure of the new compound, formulated as $Rb_{11}[\{(\beta\text{-}SiFe_2W_{10}O_{37}(OH)(H_2O)\}_2(\mu\text{-}OH)]\cdot 20H_2O\cdot 0.5RbCl$ (**Rb4**), reveals an unusual arrangement of two diiron-substituted β-Keggin tungstosilicate anions connected through an Fe−OH−Fe bridge (Figure 6). The distinction of **5** from **4** is clear: unlike **5**, **4** exhibits no ^{29}Si NMR spectrum whatsoever (even for concentrated lithiated solutions). The IR and electronic absorption spectra in the visible region of the two compounds are also distinct.

Inspection of the structure of **4** reveals that the two anionic subunits are dissymmetric positional isomers (a β(4,10) isomer and its enantiomer according to the IUPAC numbering

(44) Kurtz, J.; Donald, M. *Chem. Rev.* **1990**, *90*, 585−606.
(45) Murray, K. S. *Coord. Chem. Rev.* **1974**, *12*, 1−35.
(46) Weihe, H.; U. Güdel, H. U. *J. Am. Chem. Soc.* **1997**, *119*, 6539−6543.

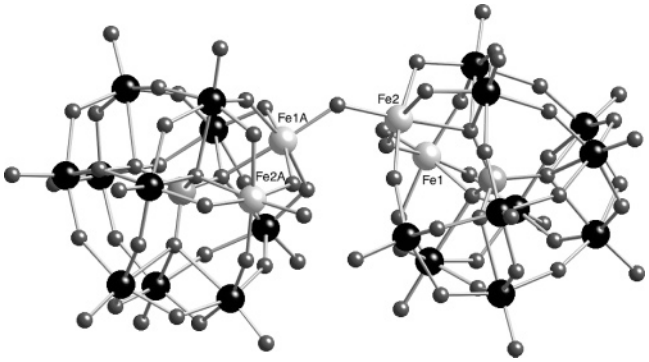

Figure 6. Structure of polyanion **4** in ball-and-stick representation: (W: large black spheres; Fe and Si: large light gray spheres; O: small gray spheres).

scheme).[47,48] All four iron centers are connected to each other by corner sharing forming an S-shaped chain. The three oxygens bridging the Fe centers have BVS values of 1.22, 1.23, and 1.38, consistent with hydroxo groups.

The relative thermodynamic stability of Keggin polytungstates is well documented to follow the order α (most stable) > β > γ.[19,49−54] In addition, since isomerization of γ-Keggin structures to β derivatives is commonly observed, it is reasonable to assume that the aging process of **2** in water involves $\gamma \rightarrow \beta$ isomerization (some details are discussed below).[49,55] The isolation and structural characterization of **4**, a β derivative, supports this assumption. In this context, Kortz and Matta noted that [γ-$SiW_{10}O_{36}$]$^{8-}$ reacts with Mn(II) cations under similar conditions to yield a C_3-symmetric trimer of β_2-[$SiW_{11}O_{39}$]$^{8-}$ units that surround a central {Mn}$_3$ core.[34d]

O_2 Oxidations by 1: Epoxidation. Mizuno and co-workers reported that O_2-based epoxidation of cyclooctene catalyzed by the tetra-*n*-butylammonium (TBA) salt of **1** proceeds in 98% selectivity and 86% conversion after ca. 400 h at 356 K in 15:1 v/v 1,2-dichloroethane/acetonitrile.[7] These are compelling numbers, but cyclooctene, unlike cyclohexene and most other alkenes, can exhibit quite high epoxidation selectivites (much lower yields of allylic oxidation products than epoxide), even under unequivocal radical chain (autoxidation) conditions. They also reported a tertiary/secondary (3°/2°) C−H cleavage ratio for reaction of adamantane, O_2, and **1** of 11 and stated that this was distinct from the conventional ratio from authentic radical reactions which "is normally three". This 3°/2° value of 3 derives from a 1967 publication on radical adamantane bromination.[56] The actual 3°/2° values from comprehensive earlier work on several radical adamantane oxidations by O_2 range from 11.6 to 16.5, with the closest conditions to Mizuno's and our reactions (AIBN + O_2) giving 16.5 (all 3°/2° values on a per C−H bond basis).[57] Mizuno and co-workers also examined 2-alkene oxidations and reported products that were stated to be distinct from those generally seen in conventional radical chain (autoxidation) processes. A concern, however, is that these ratios can vary for homolytic processes depending on the radicals present and conditions. Importantly, the authors did not report product distributions from authentic autoxidation control reactions for cyclooctene, adamantane or 2-alkenes under their conditions. Finally in their fairly thorough study, Mizuno and co-workers reported that the radical scavenger, para-*t*-butylcatechol, had little or no effect on product distributions. However, there are myriad cases where radical scavengers have no effect on radical chain processes. To inhibit a chain process, a scavenger must compete in key steps with the regular intermediates in those steps, and this is frequently not the case. Also, the efficiency of inhibition by radical scavengers is frequently proportional to radical chain length, and many metal-mediated homolytic oxidation reactions have short chains.

Given the unusually noteworthy results from this Mizuno study[7] and our desire to better understand the mechanism of this in context with the other catalytic systems for aerobic (reductant-free air-based) oxidation recently developed by our group and others, we endeavored to confirm the aerobic catalysis by **1** reported by Mizuno and co-workers using conditions identical to those in their study. Unfortunately, we found that our sample of **1** prepared following the published procedure of Mizuno et al.[6] was either not soluble or precipitated out of their reaction medium (acetonitrile/1,2-dichloroethane/alkene 0.1:1.5:2.44; see Table 1 and Figure 2 in their report). We also prepared **1** both at lower pH (additional added acid) and higher pH (added hindered pyridines) but found that these preparations of **1** exhibited the same solubility as the initial TBA**1**. As a consequence, we increased the CH_3CN/1,2-dichloroethane ratio to 1:1, at which point **1** was soluble, and we conducted all experiments in this medium. We also ran the catalyst-free control reactions in parallel. Cyclooctene oxidation was examined in some detail. Unfortunately, because the medium, and thus the catalytic system, was altered, no unequivocal inferences about the Mizuno system can be drawn.

We report the following findings. (1) The rates, conversions, and turnover number (TON) for cyclooctene oxidation with our **1** are very similar to those reported by Mizuno under their nearly equivalent (but distinct) conditions. Critically, however, the control reactions with no **1** present *proceed with similar rates and epoxidation selectivities within experimental error* to the reactions that contain **1**. (2) The product distributions from cyclohexene and 1-octene oxidations are also reproducibly the same within the experimental error of gas chromatography (capillary columns and flame ionization detectors) in the uncatalyzed (no **1** present) and catalyzed (**1** present) reactions. (3) Neither the rates nor product selectivities depend significantly on the concentration of the catalyst, **1** ([catalyst] = 0.6 mM, the same concentration as that in Table 1 of Mizuno report or 1.8 mM). (4) The selectivity, calculated as [epoxide]/([epoxide] + [alcohol] + [ketone]), is reproducibly ∼90% (typical for cyclooctene oxidation by a radical-chain process).[58,59] The 98% selectivity Mizuno and co-workers report

(47) Jeannin, Y.; Fournier, M. *Pure Appl. Chem.* **1987**, *59*, 1529−1548.
(48) Jeannin, Y. P. *Chem. Rev.* **1998**, *98*, 51−76.
(49) Canny, J.; Thouvenot, R.; Tézé, A.; Hervé, G.; Leparulo-Loftus, M.; Pope, M. T. *Inorg. Chem.* **1991**, *30*, 976−981.
(50) Weinstock, I. A.; Cowan, J. J.; Barbuzzi, E. M. G.; Zeng, H.; Hill, C. L. *J. Am. Chem. Soc.* **1999**, *121*, 4608−4617.
(51) Weinstock, I. A.; Cowan, J. J.; Barbuzzi, E. M. G.; Zeng, H.; Hill, C. L. *J. Am. Chem. Soc.* **1999**, *121*, 10856.
(52) Cowan, J. J.; Bailey, A. J.; Heintz, R. A.; Do, B. T.; Hardcastle, K. I.; Hill, C. L.; Weinstock, I. A. *Inorg. Chem.* **2001**, *40*, 6666−6675.
(53) López, X.; Maestre, J. M.; Bo, C.; Poblet, J.-M. *J. Am. Chem. Soc.* **2001**, *123*, 9571−9576.
(54) Neiwert, W. A.; Cowan, J. J.; Hardcastle, K. I.; Hill, C. L.; Weinstock, I. A. *Inorg. Chem.* **2002**, *41*, 6950−6952.
(55) Tézé, A.; Canny, J.; Gurban, L.; Thouvenot, R.; Hervé, G. *Inorg. Chem.* **1996**, *35*, 1001−1005.
(56) Tabushi, I.; Hamuro, J.; Oda, R. *J. Am. Chem. Soc.* **1967**, *89*, 7127−7129.
(57) Muto, T.; Urano, C.; Hayashi, T.; Miura, T.; Kimura, M. *Chem. Pharm. Bull.* **1983**, *31*, 1166−1171.
(58) Van Sickle, D. E.; Mayo, F. R.; Arluck, R. M. *J. Am. Chem. Soc.* **1965**, *87*, 4824−4832.

was not obtainable in our hands despite repeated attempts. (5) The mass balance, ([epoxide] + [alcohol] + [ketone])/(consumed cyclooctene), is reproducibly less than 70−80% at high conversions (Mizuno and co-workers state:[7] "The average carbon balance for six runs was 100 ± 8%"). (6) A second di-iron Keggin complex, $[\beta\text{-}SiFe_2W_{10}O_{36}(OH)_2(H_2O)Cl]^{5-}$ (**3**) with the same elemental composition and counterions (TBA) as **1**, recently characterized by several methods including a disorder-free X-ray structure,[26] was introduced to the same cyclooctene-solvent system in place of **1**. The product distribution was again the same within experimental error as that produced in the presence of **1** and in the absence of any POM.

The inescapable conclusion from all the above collective results is that the reaction with alkenes and O_2 in the presence of **1** in our hands (with **1** synthesized by the Mizuno preparation and further modified by acid or base) likely proceeds predominantly by radical-chain autoxidation. The alkene + O_2 chemistry in these organic media is minimally affected by the presence of **1**. Despite the multiple preparations of **1**, and the seeming likelihood that the complex in the Mizuno study is identical to **1**, we cannot rule out that the **1** prepared in the two laboratories may be different in some way. As a result, we cannot unequivocally rule out that their **1**, unlike our **1**, may be playing a significant role in these aerobic alkene oxidations.

O_2 Oxidations by γ(1,2)-$SiW_{10}Fe_2$ Units in H_2O: Thiol Oxidation. Although we failed to observe catalysis of selective aerobic epoxidation in organic solvents by **1**, we do find that trimer **2**, the form of the γ(1,2)-$SiW_{10}Fe_2$ unit isolable from water as described above, is a precatalyst for other aerobic oxidations in water. We focus here on oxidation of the water-soluble thiol, 2-mercaptoethanol (RSH), because the aerobic oxidation of thiols is of interest in conjunction with odor abatement, remediation, and chemical synthesis. Quantification of RSH by colorimetric methods, RSSR by ^{1}H NMR, and O_2 by volumetric methods (see Experimental section and SI) established the stoichiometry to be eq 1. Natural pH (unbuffered and controlled by POM speciation in water)[60,61] solutions were used for two reasons: first, changes in pH provide mechanistic information (pH varies from 5.5 to 7.0 during turnover), and second, three different buffers all slowed or eliminated catalytic activity even at the lowest, 20 mM, concentrations (sodium phosphate and 3-(*N*-morpholino)propanesulfonic acid, "MOPS" at pH ∼6 and sodium acetate at pH 4.5). The pK_a of 2-mercaptoethanol is 9.7.[62] Neither the reaction rates nor the yields are affected by addition of the reaction product, $(HOCH_2CH_2S)_2$. Hydrogen peroxide is not seen in the course of the reaction. It was established that H_2O_2 reacts quickly with RSH in the presence of **2** but very slowly with RSH in the absence of **2**. Three factors render eq 1 of interest in context with "green" chemistry: (i) the stoichiometry, (ii) the rate in the presence of **2** (proceeds readily at ambient temperature), and (iii) the fact that it uses the environmentally and economically optimal oxidant (O_2) and solvent (H_2O).

$$2\ HOCH_2CH_2SH + 0.5\ O_2 \rightarrow (HOCH_2CH_2S)_2 + H_2O \quad (1)$$

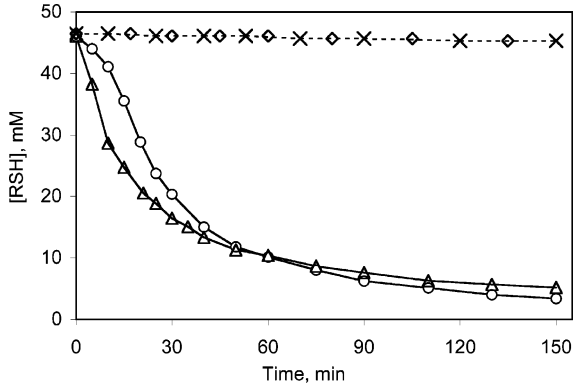

Figure 7. Kinetics of 2-mercaptoethanol (RSH) oxidation by O_2 in the absence of POMs (×) and catalyzed by 0.33 mM of $\mathbf{K_7[(CH_3)_2(NH_2)]_8 2}$ (○ − fresh, △ − aged for 15 min, ◇ − aged for 36 h). Conditions: 1 atm O_2, 24 °C, final pH ∼5.3−5.8.

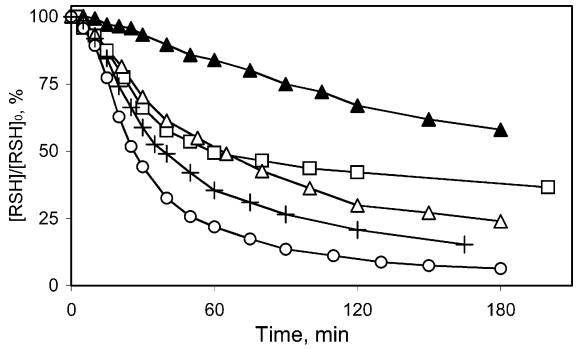

Figure 8. Effect of adding 33 and 250 mM KCl (△ and ▲, respectively), 250 mM LiCl (+), and 0.05 mM of $K_8[\gamma\text{-}SiW_{10}O_{36}]$ (□) on the rate of eq 1 (O_2-based oxidation of 46 mM RSH catalyzed with 0.33 mM of $\mathbf{K_7[(CH_3)_2(NH_2)]_8 2}$; the uninhibited catalytic reaction is marked with open circles (○)). Conditions: 1 atm O_2, 24 °C, final pH ∼5.3−5.8.

Exemplary data for RSH consumption (in eq 1) in the presence of trimer **2** are shown in Figure 7. This reaction has a short induction period if a freshly prepared solution of **2** is used but starts immediately if the solution is incubated (aged) for 10−15 min. If the solution is aged for several hours, it completely loses its catalytic activity (Figure 7). Complete conversion under the conditions in the Figure 7 caption equates to ca. 139 turnovers (initial concentrations: 46 mM of thiol and 0.33 mM of $\mathbf{K_7[(CH_3)_2(NH_2)]_8 2}$). Neither $Fe(NO_3)_3$ (natural pH ∼2.5−3.0) nor Fe^{III}(EDTA) (pH adjusted to ∼6) is active (data not shown). RSH is not consumed in the absence of **2**.

As noted above, **2** decays in unbuffered (natural pH) water, and this decay has been quantified by ^{29}Si NMR (Figure 5) and UV−visible spectra (Figure S2). Systematic studies of the decay kinetics show that the initial rates are linearly proportional to the concentration of **2**, but the reaction slows down with time (or conversion of **2**). Addition of electrolytes (KCl, LiCl, or $LiClO_4$) to aqueous solutions of **2** inhibits the decay in a concentration dependent manner. This inhibition is more pronounced for K^+ (Figure 8). Catalysis of eq 1 by solutions of **2** is also inversely proportional to the concentration of the added alkali metal salt, and this inhibition is also greater for K^+. In contrast, the rate of eq 1 catalyzed by **2** and its

(59) Van Sickle, D. E.; Mayo, F. R.; Gould, E. S.; Arluck, R. M. *J. Am. Chem. Soc.* **1967**, *89*, 977−984.
(60) Weinstock, I. A.; Barbuzzi, E. M. G.; Wemple, M. W.; Cowan, J. J.; Reiner, R. S.; Sonnen, D. M.; Heintz, R. A.; Bond, J. S.; Hill, C. L. *Nature* **2001**, *414*, 191−195.
(61) Weinstock, I.; Barbuzzi, E. M. G.; Sonnen, D. M.; Hill, C. L. In *Advancing Sustainability through Green Chemistry and Engineering*; Lankey, R. L., Anastas, P. T., Eds.; American Chemical Society: Washington, D. C., 2002; pp 87−100.
(62) *CRC Handbook of Chemistry and Physics*, 81 ed.; Lide, D. R., Ed.; CRC Press: Boca Raton, FL, 2000.

decomposition products are independent of the type of anion: alkali metal chlorides and perchlorates at similar concentrations have a comparable effect on the turnover rate. Some dependence of the rate on the solution ionic strength cannot be ruled out, but this has a less pronounced effect than the inhibitory effect of K^+. Independently, it was shown that the hydroxy-bridged dimer $Rb_{11}[\{(\beta\text{-}SiFe_2W_{10}O_{37}(OH)(H_2O)\}_2(\mu\text{-}OH)]$, **Rb4** (Figure 6), obtained by addition of Rb^+ cations to aged solutions of **2**, is completely inactive for catalyzing eq 1.

Significantly, the time- and concentration-dependent parameters all correlate with each other: the decay rate of **2** and catalysis of eq 1 and their inhibition by alkali metal cations. The catalytic system remains active for a limited time, usually less than 2−3 h. Addition of a new portion of RSH added after this time interval does not result in additional RSSR product. Also, if diluted fresh solutions of **2** are aged longer than 2−3 h in the absence of RSH and then RSH is added, no catalytic activity is present. In contrast, aging a solution of **2** for a short time (5−15 min) considerably shortens or completely eliminates the induction period. All these facts together establish that **2** decomposes in solution to form an intermediate that is the actual catalyst, and after a time, this intermediate transforms into inactive species. Such complexity makes quantifying additional aspects of the mechanism problematical. However, based on (1) the structure of the trimer, **2**, (2) the clear transformation of **2** (a compound with two types of Si in a 2:1 mole ratio) to a compound with one type of Si (cf. the ^{29}Si NMR spectra in Figure 5),[63] and (3) the similar time courses for catalyst, **2**, decomposition and decrease of catalytic activity, we conclude that a γ-SiW_{10} unit reversibly dissociates from the initial trimer to leave a more coordinately unsaturated and catalytically active $[(\gamma\text{-}SiW_{10}O_{36})_2Fe_6(OH)_9]^{7-}$ intermediate, eq 2. This catalytically active intermediate is likely to oxidize thiol to thiyl radical. The latter is further oxidized by O_2 to form $(HOCH_2CH_2S)_2$ product. The reduced Fe(II) is reoxidized by O_2 to the initial Fe(III) form. The details of the reaction mechanism will be reported elsewhere.

$$[(\gamma\text{-}SiW_{10}O_{36})_3Fe_6(OH)_9]^{15-} \rightleftarrows [(\gamma\text{-}SiW_{10}O_{36})_2Fe_6(OH)_9]^{7-} + [(\gamma\text{-}SiW_{10}O_{36})]^{8-} \quad (2)$$

To provide additional evidence for this γ-SiW_{10} dissociation mechanism, we examined the rate of eq 1 catalyzed by **2** as a function of added $K_8[\gamma\text{-}SiW_{10}O_{36}]$. Indeed, the reaction is significantly inhibited by freely diffusing γ-SiW_{10}. Furthermore, both the decay of **2** and the inhibition of the catalysis are similarly affected by addition of $K_8[\gamma\text{-}SiW_{10}O_{36}]$ (see Figure 8). Isolation of the stable and catalytically inactive β-di-iron dimer, $[\{(\beta\text{-}SiFe_2W_{10}O_{37}(OH)(H_2O)\}_2(\mu\text{-}OH)]^{12-}$, **4**, in high (ca. 70%) yield indicates that isomerization of γ isomer intermediates to beta isomer intermediates in eq 2 likely parallels loss of activity.

Conclusions

1. The $[\gamma(1,2)\text{-}SiW_{10}\{Fe(OH_2)\}_2O_{38}]^{6-}$ structure proposed for **1** forms an unsymmetrical trimer in H_2O, $[\{Fe_2(OH)_3(H_2O)_2\}_3(\gamma\text{-}SiW_{10}O_{36})_3]^{15-}$, **2**; the speciation and structure(s) of **1** in organic media remains uncertain in the absence of an X-ray structure.

2. Despite the instability of **2** in H_2O, it has been isolated and characterized by X-ray crystallography, magnetic methods, ^{29}Si NMR (which indicates the same trimer structure exists initially in H_2O), and by several other techniques. In contrast to the X-ray crystallographically characterized $[\gamma(1,2)\text{-}SiW_{10}\{Mn(OH)(OH_2)\}_2O_{36}]^{4-}$ complex and the literature structure of **1** in organic media, the three γ-di-iron-SiW_{10} Keggin units in **2** all have the two Fe^{III} centers out of the pocket (the $Fe-O_x$ bonds have been broken, and as a consequence, the Fe centers bridge, via hydroxy groups, to neighboring Fe_2 Keggin units).

3. Calculations support the observations that vicinal (adjacent) di-substituted Keggin complexes, $[\gamma(1,2)\text{-}XW_{10}\{M(OH_2)\}_2O_{38}]^{n-}$ (X, M = a heteroatom and d-electron metal center, respectively), can exist in either in-pocket (M bonded to the heteroatom oxygen, O_x) and out-of-pocket (M not bonded to the heteroatom oxygen, O_x) forms and that the existence of these two forms may be general (not limited to Cr_2 and Fe_2 derivatives only).

4. Alternatively, **2** can be viewed as a $\{Fe_6(\mu\text{-}OH)_9(H_2O)_6\}$ core stabilized by $\{\gamma(1,2)\text{-}SiW_{10}Fe_2\}$ units. The six $s = 5/2$ Fe^{III} centers are antiferromagnetically coupled to give a singlet ground state, and a best fit to an isotropic Heisenberg model results in exchange energies of $J_1/k_B = -32.5$ K, $J_2/k_B = -30.1$ K, $J_3/k_B = -39.3$ K, $J_4/k_B = -18.6$ K, and $J_5/k_B = -18.7$ K.

5. The Mizuno vicinal di-iron POM complex, $[\gamma(1,2)\text{-}SiW_{10}\{Fe(OH_2)\}_2O_{38}]^{6-}$ with in-pocket Fe(III) centers, **1**, prepared by the Mizuno method and also modified postsynthesis by addition of either acid or base has no marked effect on the reactions of alkenes and O_2 in our hands. This finding is based on several reactions with different alkenes, several control reactions, and other data including rate law determination. Despite our thoroughness and multiple failed attempts to reproduce the results of Mizuno, we cannot totally rule out that the **1** prepared by Mizuno and co-workers and its "catalytic" nonradical-chain aerobic epoxidation chemistry may be different in some way from what we document here with alkenes, O_2 and **1**.

6. Trimer **2** dissolves in aqueous solution to form an intermediate that catalyzes the effective aerobic oxidation of sulfur compounds. Mercaptoethanol oxidation in water was examined in detail to probe this chemistry. Three lines of experimental evidence are consistent with dissocation of a γ-SiW_{10} Keggin unit from the trimer, **2**, to form the catalytically active species (1) the initial structure of **2** (from X-ray crystallography); (2) the overall transformation **2** (a POM with 2 types of Si) to a POM with one type of Si; and (3) most definitively, inhibition of both the decay of **2** and the catalysis (eq 1) upon addition of γ-SiW_{10}. After a few hours and hundreds of turnovers, the catalysis ceases. Treatment of this catalytically inactive aqueous solution with Rb^+ facilitates isolation, crystallization and characterization of a hydroxy-bridged dimer, $[\{(\beta\text{-}SiFe_2W_{10}O_{37}(OH)(H_2O)\}_2(\mu\text{-}OH)]^{11-}$ (**4**), a POM in which the initial γ-Fe_2 Keggin units have rearranged to β-Fe_2 Keggin units, a finding consistent with the known relative thermodynamic stabilities of the different Baker-Figgis isomers of the Keggin structure.

Acknowledgment. We thank the Department of Energy (Grant Number DE-FG02-03ER15461) for support of this

(63) At the first glance, the decomposition of **2** (30 mM, monitored by UV−vis at 444 nm) seems to proceed faster than the formation of the final product **5** (monitored under similar conditions by ^{29}Si NMR, the resonance at −98.3 ppm). This apparent contradiction is likely due to formation of two intermediates, $[(\gamma\text{-}SiW_{10}O_{36})_2Fe_6(OH)_9]^{7-}$ and $[(\gamma\text{-}SiW_{10}O_{36})]^{8-}$. These species are not observed by ^{29}Si NMR probably due to overlapping with the signals of the initial trimer **2**.

research. Computer resources were provided in part by the Air Force Office of Scientific Research DURIP grant (FA9550-04-1-0321), the Cherry Emerson Center for Scientific Computation at Emory University, and the DOE PNNL EMSL facility under the GC3568 Grant. Ames Laboratory is operated for the U.S. Department of Energy by Iowa State University under Contract No. W-7405-Eng-82. I.W. thanks the USDA-FPL, the Graduate Research and Teaching Initiative (GRTI) of the State of New York, and PSC-CUNY.

Supporting Information Available: Additional catalytic experimental procedures, figure of **2** (Figure S1) and time dependence of the electronic spectrum of $\mathbf{K_7[(CH_3)_2(NH_2)]_8}$**2** (Figure S2), kinetic data (Figures S3 and S4), and crystallographic files for $\mathbf{K_7[(CH_3)_2(NH_2)]_8}$**2** and **Rb4** in CIF format. This material is available free of charge via the Internet at http://pubs.acs.org.

JA063157L